Title
EXTERNALLY SHUNTED JOSEPHSON JUNCTIONS: GENERALIZED WEAK LINKS

Authors
Hansma, P.K.
Sweet, J.N.
Rochlin, G.I.

Publication Date
1971-06-01

Submitted to Physical Review.

UCRL-20590 c.2

EXTERNALLY SHUNTED JOSEPHSON JUNCTIONS: GENERALIZED WEAK LINKS

P.K. Hansma, J.N. Sweet, and G.I. Rochlin

June 1971

LAWRENCE RADIATION LABORATORY
UNIVERSITY of CALIFORNIA BERKELEY

DISCLAIMER

UCRL -20590
Preprint

UNIVERSITY OF CALIFORNIA

Lawrence Berkeley Laboratory
Berkeley , California

AEC Contract No. W-7405-eng-48

EXTERNALLY SHUNTED JOSEPHSON JUNCTIONS: GENERALIZED WEAK LINKS

P. K. Hansma[†], J. N. Sweet[*], and G. I. Rochlin

June 1971

37

Externally Shunted Josephson Junctions: Generalized Weak Links

P. K. Hansma,† J. N. Sweet,* and G. I. Rochlin

Department of Physics, University of California,
and
Inorganic Materials Research Division,
Lawrence Radiation Laboratory,
Berkeley, California 94720

ABSTRACT

Using externally shunted thin film Sn-I-Sn Josephson junctions, we have experimentally verified the Stewart-McCumber predictions for the current-voltage (I-V) characteristics of a generalized weak link treated as a lumped circuit consisting of an ideal Josephson junction with critical current i_c, conductance G, and capacitance C. In addition, we have shown experimentally and theoretically that the predictions for the amount of hysteresis in the I-V characteristic as a function of the dimensionless circuit parameter $\beta_C = (\frac{2e}{\hbar})(i_c\ C/G^2)$ can be generalized to include shunt inductance, L, by replacing the capacitance with an effective capacitance $C' = C - G^2L$.

An externally shunted Josephson junction acts as a generalized weak link in that it can reproduce the behavior of other types of weak links. In fact, if the temperature of a single shunted junction is varied between 1.12K and 3.7K,

or the applied magnetic field is varied between 0 and 1 Oe, β_c can be varied over two orders of magnitude while the junction is in the cryostat. Since β_c determines the qualitative nature of the I-V characteristic this variation of β_c simulates widely different types of weak link devices. Furthermore, the accessible range of β_c for the single shunted junction can be changed while it is out of the cryostat by altering its external shunt conductance.

Thus, externally shunted Josephson junctions are theoretically well understood models of, and simulators for, the behavior of many weak-link junctions; they have the desirable property of adjustability both before and after cryostat installation. This versatility should find many significant applications.

INTRODUCTION

During the last five years, many devices have been postulated or constructed using the ac Josephson effect as their operating principle. These devices have a wide variety of applications, from ultra low-voltage galvanometers to high sensitivity radiation detectors. In physical construction they range from constricted superconducting films to (superconducting metal)-insulator-(superconducting metal) junctions.

In general these devices are known as "weak links", since the critical supercurrent in the operative portion of the device is lower than in either of the superconductors to which it is attached. This allows for local slippage of the phase of the superconductive wave function in this operative portion. The resultant phase difference across the operative portion is related to the supercurrent passing through the device; for example, in a superconducting metal-insulator-superconducting metal (S-I-S) junction, the relationship is $i = i_c \sin\phi$ where i is the supercurrent passing through the device, i_c is the "critical current", or maximum supercurrent possible, and ϕ is the difference in the phase of the superconductive wave function across the insulator. Fig. 1 shows an S-I-S thin evaporated film junction together with several other weak links of various physical construction.[1]

In 1968 Stewart[2] and McCumber[3] independently advanced a theory to explain why the observed current-voltage characteristics of one type of device (such as an S-I-S thin evaporated film junction) differed so markedly from that of other related devices (such as point contact).

They proposed that the difference between the current-voltage characteristics of such devices could be explained by a lumped circuit model that included the distributed internal resistance and capacitance of the devices in parallel with an idealized Josephson junction described by the Josephson equations.[4] Fig. 2 shows McCumber's and Stewart's theoretical results as a function of the dimensionless parameter, $\beta_C = \frac{2e}{\hbar} i_c \frac{C}{G^2}$, which gives as normalized measure of the balance of influence of the capacitance C, conductance G, and critical current i_c. Using known junction parameters it is found, for example, that ideal S-I-S thin film junctions[5] are usually in the $\beta_C \simeq \infty$ limit, small SNS junctions[6] in the $\beta_C \simeq 0$ limit, and point contacts[7,8] in the range $0 < \beta_C < 10$.

In our experiments, we modified the behavior of conventional S-I-S thin evaporated film junctions by adding an external resistive shunt in parallel with the junction. For example, one geometry we studied is shown in Fig. 3. With this shunt, the resistance that appears in the lumped circuit model of the junction is no longer simply the junction's quasiparticle tunneling resistance, but rather the parallel combination of the quasiparticle tunneling resistance and the shunt resistance. Although other workers have shunted their S-I-S thin film junctions in order to drive the junctions from a voltage source[9] or to obtain a more desirable current-voltage characteristic for their application,[10] we have performed the first systematic experimental study of the behavior of such shunted junctions for comparison with the theory of Stewart and McCumber over the entire range of β_C. In fact, we were able to investigate large

ranges of β_c for <u>each</u> shunted junction since, for these shunted junctions, β_c can be changed by applying a magnetic field or by changing the temperature, or both. For example, Fig. 4 shows the experimental results for one of our shunted junctions. Note that all the traces were made from a single such junction; β_c was externally varied.

Thus, a shunted M-I-M thin film junction behaves as a kind of generalized, tunable weak link that can be changed from one type of current-voltage characteristic to another by adjusting the temperature, the magnetic field, or both, and can be readily used to simulate or replace other, less controllable and less predictable devices in many applications.

I. THEORY

For a weak link, the equivalent lumped circuit model studied by both McCumber and Stewart is shown in Fig. 5a. The total current, I, is the sum of three terms: the current through the resistor, GV, where V is the voltage across the circuit and G is the conductance of the resistor; the current through the capacitor, C dV/dt, where C is the capacitance; and the Josephson supercurrent, $i_c \sin \phi$, where i_c is the critical current and ϕ is the difference in the phase of the superconducting wavefunction across the junction. That is:

$$I = GV + C \frac{dV}{dt} + i_c \sin \phi. \tag{1}$$

We can eliminate the voltage from the equation by using the Josephson frequency-voltage relation,[4]

$$\frac{d\phi}{dt} = \frac{2e}{\hbar} V, \tag{2}$$

thus obtaining the equation

$$I = \frac{G\hbar}{2e} \frac{d\phi}{dt} + \frac{C\hbar}{2e} \frac{d^2\phi}{dt^2} + i_c \sin \phi. \tag{3}$$

Stewart[2] and McCumber[3] independently solved this equation for the time-averaged voltage, $\langle V \rangle_t = \frac{\hbar}{2e} \langle \frac{d\phi}{dt} \rangle_t$, as a function of current, I. The qualitative nature of the solution depends on the relative magnitudes of G, C, and i_c; more specifically it depends on the magnitude of the dimensionless circuit parameter $\beta_C \equiv \frac{2e}{\hbar} i_c \frac{C}{G^2}$. Theoretical results

for various values of β_c are shown in Fig. 2. The main difference between the solutions for different values of β_c is in the amount of hysteresis in the I-V characteristic, that is, the range of current over which there is both a zero bias and a finite bias solution. Following McCumber, we can define a hysteresis parameter, α, as the ratio of the minimum current at finite voltage to the critical supercurrent. Thus α ranges from 1 in the case of no hysteresis (low β_c) to 0 in the case of maximum hysteresis (high β_c). Fig. 6 shows McCumber's results from solving Eq. (3) for α as a function of β_c.

It is easy to understand physically why β_c determines the amount of hysteresis (as measured by the hysteresis parameter α). The operative factor is whether the voltage across the junction, V, is or is not constant for times on the order of the period of the oscillation of the Josephson supercurrent. The relevant times are, respectively, $\tau_1 \equiv RC$, the capacitive circuit discharge time, and $\tau_2 \equiv \frac{\hbar}{2e} \frac{1}{i_c R}$, the inverse of the characteristic Josephson frequency. If $\tau_1 >> \tau_2$, then $\beta_c >> 1$ and the voltage across the junction is essentially constant for times on the order of the characteristic Josephson period. In this limit the time averaged contribution of the Josephson supercurrent, $i_c \sin \phi$, to the total current, I, is, using Eq. (2):

$$\langle i_c \sin \phi \rangle_t = i_c \langle \sin \frac{2e}{\hbar} Vt \rangle_t = 0 \qquad (4)$$

at any finite voltage V. Thus there is no net dc supercurrent flowing at finite voltage in this limit. Similarly, there is no time averaged current from the capacitive channel, $C \frac{dV}{dT}$. Consequently, the only

current flowing at finite voltage is the ohmic current, GV. Since this ohmic current goes to zero as the voltage goes to zero, we have maximum hysteresis, implying that in the limit $\beta_C >> 1$, $\alpha = 0$.

If, on the other hand, $\tau_1 < \tau_2$, so that $\beta_C < 1$, then the capacitance is not large enough to keep the voltage across the junction constant for times on the order of the period of the Josephson supercurrent and we must do our averaging more carefully. For simplicity, consider the limit in which there is no capacitance, $C = 0$, so the capacitive discharge time is zero and $\beta_C = 0$. Then Eq. (3) becomes

$$\frac{d\phi}{dt} = \frac{2e}{\hbar G} (I - i_c \sin \phi). \qquad (5)$$

We can easily see that for $I > i_c$ and $\sin \phi > 0$, ϕ is changing less rapidly than it is for $\sin \phi < 0$. Since $\sin \phi$ is thus positive longer than it is negative, the time averaged Josephson supercurrent $\langle i_c \sin\phi \rangle_t$, is greater than zero. Hence, a finite net dc supercurrent flows at finite voltages and the total current, I, no longer goes to zero as V approaches zero as it did for the previous case. That is, $\alpha > 0$ for small β_C. The conclusions of these simple physical arguments are shown to be correct by the detailed solution for α vs β_C (Fig. 6).

A difficulty in applying this theory to unshunted S-I-S thin film tunneling junctions is that the effective distributed conductance is due to quasiparticle tunneling which is strongly voltage-dependent. This consideration implies that the voltage-independent conductance of the theory, G, must be replaced by a voltage-dependent conductance G(V).[11] For our shunted

junctions, however, this is not a problem since the shunt conductance, which is independent of voltage, is much larger than the quasiparticle tunneling conductance. Hence, the total conductance is very nearly independent of voltage, as required by the theory.

There is, however, a significant difference between the equivalent circuit for many of our shunted junctions and the equivalent circuit of the theory (Fig. 5a). In particular, for shunted junctions of the geometry shown in Fig. 3, there is a non-negligible inductance in the loop formed by the shunt and the junction leads; Fig. 5b is the equivalent lumped circuit. For this circuit the complex impedance seen by the junction is, in general, different from that studied by McCumber and Stewart. But, in the limit $V \to 0$ it has exactly the same form, with C replaced by an effective capacitance $C' = C - G^2L$. Let us consider the complex impedance seen by the junction in the circuit of Fig. 5a. Since it is fed by a current source, which is driven with essentially infinite impedance, we need only consider the contributions from the circuit elements shown in Fig. 5a, which will have the form,

$$Z(\omega) = (i\omega C + G)^{-1}. \tag{6}$$

For the circuit shown in Fig. 5b, this impedance becomes:

$$Z(\omega) = \left(i\omega\left(C - \frac{G^2L}{1+(\omega GL)^2}\right) + \frac{G}{1+(\omega GL)^2}\right)^{-1}. \tag{7}$$

It can be seen that for low frequencies, $\omega << \frac{1}{GL}$, Eq. (7) has the same form as Eq. (6) with C replaced by $[C - G^2L]$. Thus, in the limit where the frequency of the Josephson oscillations becomes small, that is in the limit $V \to 0$, we recover the complex impedance studied by McCumber and Stewart. Fortunately, it is in this $V \to 0$ limit that α and β_c are determined. Consequently, McCumber's results for the hysteresis parameter, α, as a function of the circuit parameter β_c should still apply with the replacement noted above:

$$\beta'_c = \frac{2e}{\hbar} i_c \frac{C - G^2L}{G} . \qquad (8)$$

The final useful generalization of the theory is the consideration of the effect of a magnetic field in the plane of the junction. In this case the difference is superconducting phase across the junction, ϕ, is no longer a constant but varies spatially across the junction. However, this generalization proves trivial since Eq. (3) contains no spatial dependence, only differentiation with respect to time. Consequently, if we use it as a local equation for the current density, $j(x)$, as a function of the local difference in superconducting phase across the junction, $\phi(x)$, we can formally integrate over the area of the junction and then interchange this spatial integration with the time differentiations. For the case of experimental interest in which the magnetic field, H, is applied parallel to one side of the oxide barrier, the resultant equation is ,

$$I = \frac{\hbar G}{2e}\frac{d\phi_o}{dt} + \frac{\hbar C}{2e}\frac{d^2\phi_o}{dt^2} + i'_c \sin\phi_o \qquad (9)$$

where ϕ_o is the average difference in superconducting phase across the junction and

$$i'_c = i_c \frac{\sin(\frac{2edW}{\hbar c} H)}{(\frac{2edW}{\hbar c} H)} \qquad (10)$$

where W is the width of the oxide barrier and $d = 2\lambda + \ell$, where λ is the effective penetration depth and ℓ is the insulator thickness.[12] Thus, in the presence of a magnetic field the resultant equation for the current has exactly the same form as Eq. (3) with the difference in superconducting phase across the junction, ϕ, replaced by the average difference in superconducting phase across the junction, ϕ_o, and the critical current, i_c, replaced by the reduced critical current i'_c. Consequently the shape of the current voltage characteristics depend on the magnetic field only through the effect of reducing the critical current.

EXPERIMENTAL METHODS

A. Sample Preparation

The shunted Sn-SnO-Sn junctions used in our experiments were prepared by vacuum deposition of thin metallic strips onto microscope cover glass substrates 1.3×10^{-2} cm thick. The widths of the strip electrodes being deposited were delineated by thin aluminum masks located directly below the substrates. Evaporation pressures were in the range $(2\text{-}50) \times 10^{-7}$ Torr and evaporation rates were in the ranges

5-10 Å/sec. There was no observable correlation between final junction quality and evaporation pressures or rates. All evaporations were performed at room temperature in an ion-pumped high vacuum system.

For the samples shown in Fig. 3, 1.5 mm wide Ag strips 500 - 5,000 Å thick were deposited first to act as the normal shunts. Next, a 0.18 mm wide longitudinal Sn strip 3,000 Å thick, was deposited and then oxidized in pure oxygen at a pressure of approximately 1/3 atm. The oxidation time was varied from 12 - 36 hours and the oxidation temperature was controlled with heat lamps. Following oxidation of the bottom electrode, three 0.18 mm wide Sn cross strip top electrodes were deposited in a perpendicular direction so as to form two shunted and one unshunted crossed strip tunnel junctions on the same substrate. In addition, we constructed many samples of other geometries to reduce the loop inductance present in the above geometry. The most successful type consisted of a Sn-SnO-Sn junction as described above, but with a small Ag rectangle evaporated directly on top of the completed junction, replacing the Ag strip.

In general, for junctions with an area 0.18×0.18 mm^2, a 12-hour oxidation at 300K would produce Sn-SnO-Sn junctions with 4.2K normal state resistances in the milliohm range, while a 24-hour oxidation using two heat lamps (standard 250 W infrared flood lights, approximately 3 ft. from the oxidation belljar) would produce resistances in the range 2 - 10 Ω.

In addition to these shunted junctions, two very high resistance unshunted Sn-SnO-Sn junctions were produced for capacitance measurements. These junctions were oxidized for over one month with two heat lamps

approximately 3 ft. from the oxidation belljar. They had resistances of 1,000 Ω and 1,900 Ω. Attempts to produce high resistance junctions using higher temperatures for shorter times or glow discharge oxidation produced shorted junctions.

Following completion of the sample, it was installed in the sample holder and electrical leads were attached with silver paint. In general, the samples were installed and cooled down to liquid nitrogen temperature within 30 - 60 minutes after completion of the final deposition.

B. Electronics

The tunnel junction I-V characteristics were displayed on an X-Y oscilloscope by sweeping the junction with a constant current sawtooth supplied by a signal generator in series with a large resistor (> 1000 times the sample resistance). A typical frequency of the current sweep was 200 Hz. The voltage across the sample was first amplified by a low-noise, floating differential amplifier and then applied to the oscilloscope's X axis. The voltage across a 100 Ω resistor in series with the constant current supply was applied to the oscilloscope's Y axis. The resultant I-V traces were photographed with an oscilloscope camera and the measurements performed later on these photographs.

C. Measurements

The two quantitative predictions of the theory are the dependence of the hysteresis, as measured by the hysteresis parameter α, on the circuit parameter β_C and the shape of the I-V curves. The shape of the

I-V curves could be measured directly from the photographs or, alternately, from x-y chart recordings made with slower current sweeps (~ 0.1 cps). Our primary interest was in verifying the α vs β_C curve. We varied β_C by changing i_c with magnetic field or temperature (recall $\beta_C = \frac{2e}{\hbar} i_c \frac{C}{G^2}$). For each value of i_c, a photograph was taken. From these photographs, we could measure i_c, G, and α. The effective capacitance was determined by fitting one point (usually the point of largest i_c) on the β_C vs α curve. Then, using this value of capacitance, we could evaluate β_C for all of the other photographs and plot β_C vs α as a series of points, each point corresponding to one photograph. The effect of varying C is to move all the experimental points uniformly up or down since β_C is plotted on a log axis (see Fig. 7, 8, and 9). Thus, data from each sample were fitted to the theoretical curve with the single adjustable parameter, C.

EXPERIMENTAL RESULTS

A. Comparison with Theory

For the junctions of the geometry shown in Fig. 3, the loop inductance is not negligible; that is, the correction term G^2L is smaller than, but comparable to, the junction capacitance, C. Consequently, only the $V \to 0$ behavior will be quantitatively explained by the theory. However, β_C and α are both determined only by this $V \to 0$ behavior; β_C is dependent on the zero bias supercurrent and α is dependent on the zero bias supercurrent together with the $V \to 0$ limit of the current flowing at finite voltage. Therefore, these

junctions should show good agreement with the theoretical predictions for α as a function of β_C.

Figs. 7, 8, and 9 show the experimental results as points; the solid line is the theory (Fig. 6). The only effect of the loop inductance is to lower the fitting capacitance $C' = C - G^2L$ from the true capacitance, C. In particular, the values of fitting capacitance for these figures were 240 pF, 110pF, and 140 pF respectively; the true capacitance (see experimental section B) is approximately 500 - 600 pF for these junctions.

The finite voltage behavior of these shunted junctions is indeed different from that predicted by the theory. Though the detailed behavior varied somewhat from sample to sample as G^2L varied, the general behavior can be characterized as more nearly ohmic than in the L = 0 case. This effect is easily understood qualitatively by using Eq. (7) together with Fig. 2. From Eq. (7) it can be seen that the effective capacitance, $C'(\omega) = \{C - G^2L\,[1 + (\omega GL)^2]^{-1}\}$, increases for increasing ω. As the average voltage across the junction increases, the frequency of the ac Josephson current also increases. Consequently, the junction sees a higher effective capacitance at finite voltage than at zero voltage. It is this higher effective capacitance, resulting in a higher effective value of β_C, that makes the finite voltage part of the current-voltage traces more nearly ohmic. This can be seen immediately by comparing the limit of large effective capacitance $\beta_C \to \infty$, where the finite voltage part of the current-voltage trace is ohmic all the way to the origin; with the limit of small effective capacitance $\beta_C \to 0$, where the finite voltage part of the current-voltage trace shows maximum deviation from ohmic

(see Fig. 2a,b).

In order to test the hypothesis that loop inductance was responsible for the deviation from theoretical predictions, we constructed a series of samples of different geometries designed to minimize that inductance. The experimental results for a sample of the most successful geometry are shown in Fig. 4. For this type of sample the Josephson junctions were similar to those shown in Fig. 3 except that a small Ag rectangle evaporated directly on top of the completed junctions replaced the Ag strip. This Ag rectangle completely covered the junction and extended slightly beyond it (~ .1 mm) on either side to form two Ag-SnO-Sn quasiparticle tunneling junctions that acted as the shunts. Because the shunting was through quasiparticle junctions, data could be taken only at temperatures near enough to T_c so that the quasiparticle conductance was linear over the range of voltage bias studied. Experimentally, temperatures on the order of 3.2K were sufficient to give a linear conductance to within a few per cent from 0 to 100 uV. Furthermore, the quasiparticle tunneling junctions contributed to the capacitance of the Josephson tunneling junction, making comparisons of the fitting capacitance vs Josephson junction capacitance meaningless except to note that the fitting capacitances are indeed larger (~ 800 pf) than the Josephson junction capacitance (500 - 600 pf). If the quasiparticle junctions were eliminated by evaporating the silver rectangle under the Josephson junction then S-N-S junctions, with critical currents comparable to the Josephson junction's critical current, were formed directly at either side of the Josephson junction. These S-N-S junctions eliminated the possibility of any quantitative measurements in the same way as microshorts, to be discussed in a

later section. Another way of minimizing loop inductance is to evaporate a superconducting ground plane over the entire sample, separated from it by a thin insulating layer.

For applications in which the detailed shape of the finite voltage part of the characteristic is not important, the geometry shown in Fig. 3 has two significant advantages over any of the lower inductance geometries. First, the lower effective capacitance is useful for applications requiring a high critical current with no hysteresis in the current-voltage characteristic ($\alpha = 1$), since for a given G, the necessary low value of β_c can be obtained at larger critical current i_c. These larger critical currents are often useful in practical applications since they can be measured with greater precision. A second advantage is that the shunt conductance can be easily varied after the sample is completed; it can be lowered by scraping away part of the silver film, or it can be increased by adding silver paint. This capability is very desirable since it allows the experimenter to fix the value of β_c that corresponds to the junction's maximum critical current (i_c at the lowest attainable temperature in zero magnetic field) at any value convenient for his experiment. In fact, we made extensive use of this ability in our experiments. In particular, after all data were taken with a given shunt, and if the sample was still good, it was warmed to room temperature rapidly by heating it with a heat lamp. The shunt resistance was then changed to whatever new value was desired (as described above), and the sample re-cooled.

For example, one sample, 113A, was raised to room temperature to have its shunt conductance changed five times with no noticeable decrease in

sample equality (as measured by its magnetic field diffraction pattern). Between experimental runs it was stored at liquid nitrogen temperature in He gas. Figs. 8, 9, and 10 show the experimental results for three different shunt conductances, 47 mho, 13.5 mho, and 2.8 mho respectively. In addition, for one experimental run the shunt was completely scraped away. The resultant unshunted junction had excellent S-I-S superconducting tunnel junction characteristics; the excess conductance below the superconducting energy gap 2Δ was less than 1/2 of 1% of the normal state quasiparticle conductance.

B. Junction Capacitance

From the Fiske mode positions in our junctions,[13] we could get a crude estimate of the true junction capacitance by assuming that the penetration depth in the junction, λ, was approximately equal to the bulk value 510 Å.[14] The observed Fiske mode position of 115 ± 5 μV gives a capacitance estimate of 615 ± 50 pF. We could get a better estimate from the two high resistance junctions mentioned earlier; their capacitance could be measured directly by using a capacitance bridge since for these high resistance junctions the dynamic resistance for voltages below 1 mV was as high as 2×10^5 Ω, giving a resistive conductance of 5×10^{-6} mho. If we operated the capacitance bridge at a frequency of 5000 Hz the capacitive conductance, C, was approximately 1.2×10^{-5} mho, on the order of the resistive conductance, thus and could be measured by the capacitance bridge. The measured value of capacitance for this junction was approximately 400 pF. For smaller resistance junctions, such as those used in our β_c vs α measurements, the capacitive conductance was negligible relative to the resistive conductance;

consequently, the capacitance could not be measured directly.

Furthermore, because of the high junction resistance we were able to plot current-voltage curves out to over one volt in bias. From these curves we could estimate the barrier height from Fowler-Nordheim plots.[15] These estimates were still somewhat crude since even voltages over one volt are not high enough to get into the true Fowler-Nordheim region, but we could determine that the barrier height, Φ, was greater than .5 eV and less than .8 eV by using the value of barrier thickness d, obtained from the standard formula for the capacitance, C, of two parallel plates of area, A, separated by an insulating layer of thickness ℓ, and dielectric constant, ε,

$$C = \frac{\varepsilon A}{\ell}, \quad \text{(MKS)} \tag{9}$$

with $4 < \varepsilon/\varepsilon_o < 5$,[16] $A = 3.24 \times 10^{-8}$ m^2, and C = 400 pF. We could then extrapolate the capacitance for these high resistance junctions down to that for the lower resistance junctions used in our research. This was done using Eq. (9) together with the approximate theoretical result for the resistance, R, of an S-I-S tunneling junction as a function of the barrier height, Φ, and thickness ℓ of the insulating layer,

$$R \propto \exp\left(\frac{2(2m\Phi)^{1/2}}{\hbar}\,\ell\right). \tag{10}$$

With ranges of $4 < \varepsilon/\varepsilon_o < 5$ and .5 eV < Φ < .8 eV, the extreme values of capacitance, extrapolated from the measured value of 400 pF at 2,000Ω, were 508 pF < C < 602 pF for a 2Ω junction. Combining this

with the uncertainty in the measurement of the 400 pF we obtain the final result that the capacitance of the tunneling junctions used in our research was 555 ± 90 pF, which is consistent with the Fiske mode estimate of 615 ± 50 pF. In addition, this Fiske mode estimate is based on the assumption that penetration depth in the junction is the bulk value; an assumption of a larger penetration depth would lower the estimate. Thus, for a junction with a specific normal state resistance, $r_n = 6.5 \times 10^{-8} \Omega\text{-m}^2$ we find an experimental value of $\ell\, \varepsilon_o/\varepsilon = 5.2 \pm 1$ Å.

CURRENT NOISE, MICROSHORTS, AND FISKE MODES

As with any device of this type, we must carefully take into account the effects of current noise, microshorts, and Fiske modes. For junctions in which any of these is significant, the qualitative behavior remains the same (α increases as β_C is decreased), but the quantitative agreement with McCumber's theory is degraded, in some cases substantially so.

A. Current Noise

For currents, I, in the range $\alpha i_c < I < i_c$ there are two voltage solutions, one at finite voltage and one at zero voltage (Figs. 2 and 4). Experimentally, we found that near αi_c the zero voltage solution was more stable and that near i_c the finite voltage solution was more stable. For example, if a shunted junction was biased at a constant current near i_c, noise spikes would cause transitions from the zero voltage solution to the finite voltage solution but never back again.

Our measurements of α vs β_C depend on measurements of i_c and αi_c from oscilloscope photographs of voltage as a function of bias current. That is, the measured value of i_c is the bias current at which the jump to finite voltage from zero voltage occurs and the measured value of αi_c

is the bias current at which the reverse jump occurs. If we assume that the total current through the junction consists of the sum of the bias current plus a small rapidly varying noise current, the observations on the relative stability of the zero voltage and finite voltage solutions at various currents leads to a simple prediction: the measured value of i_c will be too low and the measured value of αi_c will be too high.

That is, the total current will momentarily exceed i_c before the bias current reaches it because of the rapidly varying noise current. For a total current greater than i_c, the only stable solution is the finite voltages one, and a transition will be made. Once at the finite voltage solution the shunted junction will not make the transition back to the zero voltage solution even though the total current drops below i_c (as the noise current fluctuates) because the finite voltage solution is more stable near i_c. Similarly, as the bias current is being decreased the transition back to the zero voltage solution will occur slightly before αi_c.

Let us define δi_c as the difference between the actual value of i_c and the measured value from the oscilloscope photograph and $\delta(\alpha i_c)$ as the difference between the actual value of αi_c and the measured value. δi_c and $\delta(\alpha i_c)$ will both be on the order of one-half the peak-to-peak noise current). The simplest assumption is that $\delta i_c = \delta(\alpha i_c) = \delta i$ and that they are independent of the magnitude of i_c for a given sample at a given time. Then the measured value of the hysteresis parameter, defined as $\alpha^{(ms)}$ will be:

$$\alpha^{(ms)} = \frac{\alpha i_c + \delta i}{i_c - \delta i} \qquad (11)$$

Since β^c is proportional to i_c, we will have a measured value, defined as $\beta^c_{(ma)}$ or

$$\beta^c_{(ma)} = \beta^c \cdot \frac{(i_c - gi)}{i_c} \qquad (12)$$

For a shunted junction with effective capacitance C and shunt conductance G we can plot these theoretical predictions for various values of current noise by eliminating i_c from the above equations using the definition of β^c. Then the equations become:

$$\alpha_{(ma)} = \frac{1 - gi'/\beta^c}{\alpha + gi'/\beta^c} \cdot \qquad (11')$$

$$\beta_{(ma)} = \beta^c(1 - \frac{\beta^c}{gi'}), \qquad (12')$$

in which gi' is a normalized current noise defined as:

$$gi' = \frac{\pi G_S}{2ecgi} \cdot \qquad (13)$$

We may now compare the theoretical predictions of this simple model to experimental results. The left graph of Fig. 10 shows a theoretical plot of $\alpha_{(ma)}$ vs $\beta^c_{(ma)}$ for various arbitrary values of current noise, gi', made using Eqs. (11'), (12'), and (13). First, for each value of current noise, the <u>effective</u> current noise, gi', was computed using Eq. (13) and the value of C/G_S for the sample shown in the right graph of Fig. 10. Then, the plot of $\alpha_{(ma)}$ vs $\beta^c_{(ma)}$ was made for each value of effective current noise by using Eqs. (11') and (12') together with the theoretical

curve of α vs β_c (Fig. 6).

The right graph of Fig. 10 shows the experimental results for the effects of various naturally occurring and induced levels of current noise. Note that the naturally occurring level of current noise is lower at night than during the day (our laboratory is directly over the main machine shop for the Physics Department). In addition to observing the effects of various naturally occurring levels of current noise, we observed the effect of an artifically induced, larger current noise by applying a 4 GHz microwave signal to the sample in a rectangular cavity operating in the TE_{101} mode.[6] For example, one of the curves in this figure shows the effect of applying 6×10^{-6} W of microwave power.

To reduce these effects, one must reduce the effective noise current given by Eq. (13). This can be done either by reducing the actual noise current through more careful shielding or, more simply, by increasing the shunt conductance, G. For example, Figs. 8 and 9 show the same sample as in Fig. 6b for higher values of shunt conductance but the same actual value of current noise δi. The physical basis of this effect is simple: for larger shunt conductances more of the noise current flows through the shunt and less through the junction. This may well have important applications for devices in which current noise presently limits the resolution.

B. Microshorts

A microshort can be readily detected by plotting a Josephson junction's critical current, i_c, vs magnetic field and examining the resulting diffraction pattern. Several diffraction patterns for

our junctions are shown in Figs. 11a,b; they have well-defined zeros at all the minima. For junctions with diffraction patterns that do not have such well-defined zeros, microshorts are suspected which will distort the measured α vs β_C curve. A simple model for predicting the effect of a microshort on a measured α vs β_C curve assumes that a microshort of critical current i'_c has a current voltage characteristic similar to that of a microbridge; that is, like the $\beta_C = 0$ curve of Fig. 2a,b. Assuming that the total current flowing at any bias through the shunted junction with a microshort is simply equal to the sum of the current through an ideal shunted junction plus the current through the microshort, we can immediately write:

$$\alpha^{(ms)} = \frac{\alpha i_c + i'_c}{i_c + i'}$$

$$\beta_C^{(ms)} = \beta_C \frac{i_c + i'_c}{i_c} .$$

Thus, the effect of a microshort is to increase the measured values of both α and β_C from what they would be for the same junction without the microshort. Hence, the effect on the α vs β_C curve is to move the measured points, $(\alpha^{ms}, \beta_C^{ms})$ above the values for the unshorted junction, (α, β_C). The larger the microshort's critical current, i'_c, relative to i_c the larger this shift will be. Furthermore, since the temperature and magnetic field dependence of the critical current of a microshort is not the same as that of a M-I-M tunneling junction, when we vary β_C by varying the magnetic field or the temperature, the amount of the shift of $(\alpha^{(ms)}$ vs $\beta_C^{(ms)})$ will vary, and

the measured α vs β_c curve will not only be shifted, it will also be distorted.

In light of the above considerations, we carefully checked the critical current, i_c, vs magnetic field diffraction pattern of each sample before and after taking data. All data published in this report were obtained from samples for which there was zero current, to the resolution of our apparatus ($\Delta i_c/i_c \simeq 10^{-3}$) at any of the minima.

C. Fiske Modes

In some of our earlier junctions Fiske modes interfered with accurate measurement of the α vs β_c curve. As mentioned in the section on current noise, for currents near αi_c the zero voltage solution is more stable than the finite voltage solution. If this current αi_c was slightly less than the current at the top or bottom of a Fiske mode, we observed premature transitions to the zero voltage solution from the Fiske mode.

It was possible, however, to construct samples in which these premature transitions never occurred by adjusting the sample's current-voltage characteristic so that the currents corresponding to the first Fiske mode were much greater than the largest value of αi_c. In these samples the Fiske modes were in a current range for which the finite voltage solution was stable. Consequently, no premature transitions to the zero voltage solution occurred. In fact, in some samples, the currents at the first and, consequently, at all higher order Fiske modes were higher than the critical current, i_c. Obviously, for these samples, no transitions to a zero voltage solution from a Fiske mode could occur since there was no zero voltage

solution at the corresponding currents.

As mentioned in the section on junction capacitance, the first Fiske mode occurred at 115 ± 5 μV in our samples. Consequently, the currents corresponding to the first Fiske mode were on the order of the shunt conductance, G, times 115 μV. Assuming that we wished to start our α vs β_C plot at some fixed value of β_C, the definition of β_C shows that, for fixed capacitance, we needed to make i_c proportional to G^2. Consequently, the ratio of i_c to the currents corresponding to the first Fiske mode was proportional to G. Thus, by lowering G and raising the junction's normal state resistance to lower i_c in such a way that the ratio i_c/G^2 stayed fixed, we could eliminate the problem of premature transitions caused by Fiske modes.

Even, however, for our early junctions in which Fiske modes were a problem, we were able to make accurate α vs β_C measurements. These measurements were possible since the Fiske modes in all our junctions are very small or, more often, nonexistent in zero magnetic field. Consequently, β_C could be varied with temperature in zero magnetic field, even though it could not be varied with magnetic field. For example, Fig. 7 shows our experimental results for α vs $\beta_C(T)$ for a junction in which the maximum value of αi_c was greater than current corresponding to the third Fiske mode. As the critical current, i_c, was decreased with temperature in zero magnetic field, αi_c decreased smoothly through the currents corresponding to the third, second, and first Fiske modes respectively; the Fiske modes did not appear.

SUMMARY

By analyzing the behavior of externally shunted ideal Josephson junctions, we have determined that the models of Stewart and McCumber, which analyze a generalized weak link as an idealized junction with distributed internal resistance and capacitance are valid approaches. Thus the widely varying current-voltage characteristics of many of the weak-link Josephson devices in the literature may not only be analyzed in terms of such a model, but also simulated easily and reproducibly in the laboratory.

The predictions of these theories for the hysteresis parameter, α, which measures the ratio of the minimum current intercept of the finite voltage characteristic with the current axis at zero voltage to the maximum critical current as a function of the dimensionless circuit parameter, $\beta_C = (\frac{2e}{\hbar}) i_c \frac{C}{G^2}$, have been directly verified by measurements on such externally shunted junctions. We have also generalized the theory somewhat to treat, experimentally and theoretically, two extensions of the basic case discussed by Stewart and McCumber.

For the case in which the junction capacitance and shunt inductance are both significant, the theoretical predictions for α as a function of β_C have been extended to include the inductance by replacing the capacitance, with an effective capacitance $C' = C - G^2L$. The finite voltage portion of the characteristic for this case is solvable in principle by numerical methods, but we have made no attempt to do so here. We merely note the fact that the characteristic becomes more nearly ohmic at finite voltages as the ratio of G^2L to C increases.

We have also extended the model to the case of a particular

spatially varying phase difference, the case of a non-self-field-limited junction in a homogeneous magnetic field parallel to the surface. Our results reduce to those of McCumber and Stewart as the magnetic field goes to zero.

In addition to providing experimental verification of the lumped circuit models of weak links, these externally shunted junctions are tunable in a predictable way simply by increasing or decreasing the shunt conductance, or changing the temperature and or magnetic field.

For example, most device applications of weak links depend on the measurement of variations in their critical current. In the range of no hysteresis ($\alpha = 1$) this can be simply done by biasing at a current just above the critical current and measuring the voltage variations $\Delta V = R_d \Delta i_c$ where R_d, which determines the sensitivity, is the dynamic resistance at the operating current. In an externally shunted junction, R_d, and hence the sensitivity can be easily adjusted both before and after cryostat installation by any of the methods mentioned above. Due to their versatility, externally shunted Josephson junctions may well find applications in areas where other, less controllable, less reliable, and non-adjustable weak links have been used, or in cases where the performance of a device must be altered in mid-experiment to provide optimum instrumental sensitivity.

In short, what we have constructed and analyzed is a simple, reproducible, reliable, and theoretically well understood Josephson junction device with the desirable properties of adjustability both before and after cryostat installation. At present these serve as

models of, and simulators for, the behavior of many weak-link junctions; they have the potential of replacing less versatile devices in applications of the Josephson effect for sensitive detection of voltage, current, and infra-red radiation.

ACKNOWLEDGEMENTS

We wish to acknowledge many helpful discussions with Dr. John Clarke.

This work was performed under the auspices of the U. S. Atomic Energy Commission.

REFERENCES

† National Science Foundation Research Fellow.

* Present address: Sandia Laboratories, Albuquerque, N.M. 87059

1. Fig. from J. Clarke, Am. J. Phys. 38, 1071 (1970).
2. W. C. Stewart, Appl. Phys. Letters 12, 277 (1968).
3. D. E. McCumber, J. Appl. Phys. 39, 3113 (1968).
4. B. D. Josephson, Phys. Letters 1, 251 (1962); Rev. Mod. Phys. 36, 216 (1964); Advan. Phys. 14, 419 (1965).
5. P. W. Anderson and J. M. Rowell, Phys. Rev. Letters 10, 230 (1963).
6. J. Clarke, Proc. Roy. Soc. A308, 447 (1969).
7. J. E. Zimmerman and A. H. Silver, Phys. Rev. 141, 367 (1966).
8. L. J. Barnes, Phys. Rev. 184, 434 (1969).
9. S. A. Buckner, J. T. Chen, and D. N. Langenberg, Phys. Rev. Letters 25, 738 (1970).
10. P. W. Anderson, R. C. Dynes, and T. A. Fulton, Bull. Am. Phys. Soc. Series II, 16, 399 (1971).
11. W. C. Scott, Appl. Phys. Letters 17, 166 (1970).
12. Eq. (10) is based on the assumption of a uniform oxide layer. See R. C. Dynes and T. A. Fulton, Phys. Rev. B 3, 3015 (1971).
13. D. Coon and M. Fiske, Phys. Rev. 138, A744 (1965).
14. A. J. Dahm, A. Denenstein, T. F. Finnegan, D. N. Langenberg, and D. J. Scalapino, Phys. Rev. Letters 20, 859 (1968).
15. See, for example, J. E. Christopher, R. V. Coleman, A. Isin, and R. C. Morris, Phys. Rev. 172, 485 (1968).
16. This is the range of ε that has been assumed by previous researchers for thin film tin oxide. We know of no direct measurement.

FIGURE CAPTIONS

Fig. 1. Various weak links.[1] (a) Superconductor-Insulator-Superconductor (S-I-S) thin film tunneling junction; (b) Superconductor-Normal Metal-Superconductor (S-N-S) thin film tunneling junction; (c) Dayem bridge; (d) Notarys-Mercereau bridge; (e) Crossed wires; (f) point contact; (g) Slug.

Fig. 2. (a) McCumber's theoretical results for the voltage vs current of a weak link as a function of the dimensionless circuit parameter, β_c; (b) Stewart's theoretical results (In the original paper,[3] Stewart labeled his curves with his own dimensionless parameter $\omega_o\tau$, which is equal to $(\beta_c)^{(1/2)}$.

Fig. 3. One type of externally shunted Josephson junction used in our experiments. Two of the three S-I-S Josephson junctions formed at the intersections of the tin films are shunted with silver strips.

Fig. 4. Experimental results for the voltage vs current of an externally shunted Josephson junction as a function of the dimensionless circuit parameter β_c.

Fig. 5. (a) The equivalent lumped circuit model of a weak link studied by both McCumber and Stewart; (b) The equivalent lumped circuit model for the type of externally shunted Josephson junction shown in Fig. 3.

Fig. 6. McCumber's theoretical results for the hysteresis parameter, α, as a function of the circuit parameter, β_c.

Fig. 7. Experimental results for the hysteresis parameter, α, as a function of the circuit parameter β_c. The circuit parameter was varied by changing the temperature from 1.12K for the uppermost

point to within a few mK of the transition temperature, 3.7K, for the lowest point. The solid curve is the theoretical prediction (Fig. 6).

Fig. 8. Experimental results for the hysteresis parameter, α, as a function of the circuit parameter β_c. The circuit parameter was varied by changing the temperature from 1.12K to 3.6K.

Fig. 9. Experimental results for the hysteresis parameter, α, as a function of the circuit parameter β_c. This is the same junction as in Fig. 8 with its shunt conductance reduced. The circuit parameter was varied both with temperature (1.12K → 3.7K) and with magnetic field (0 → 1 G).

Fig. 10. The left graph shows the theoretical results of Eqs. (11'), (12'), and (13) for the effect of current noise on the measured α vs β_c curve. The right graph shows the experimental results for the effect of various natural and artificially-induced levels of current noise. The junction is the same as in Figs. 8 and 9 with its shunt conductance further reduced. The circuit parameter was varied with magnetic field (0 → 1 G).

Fig. 11. (a,b) The maximum Josephson current, i_c, as a function of magnetic field for samples 109C and 113A, respectively.

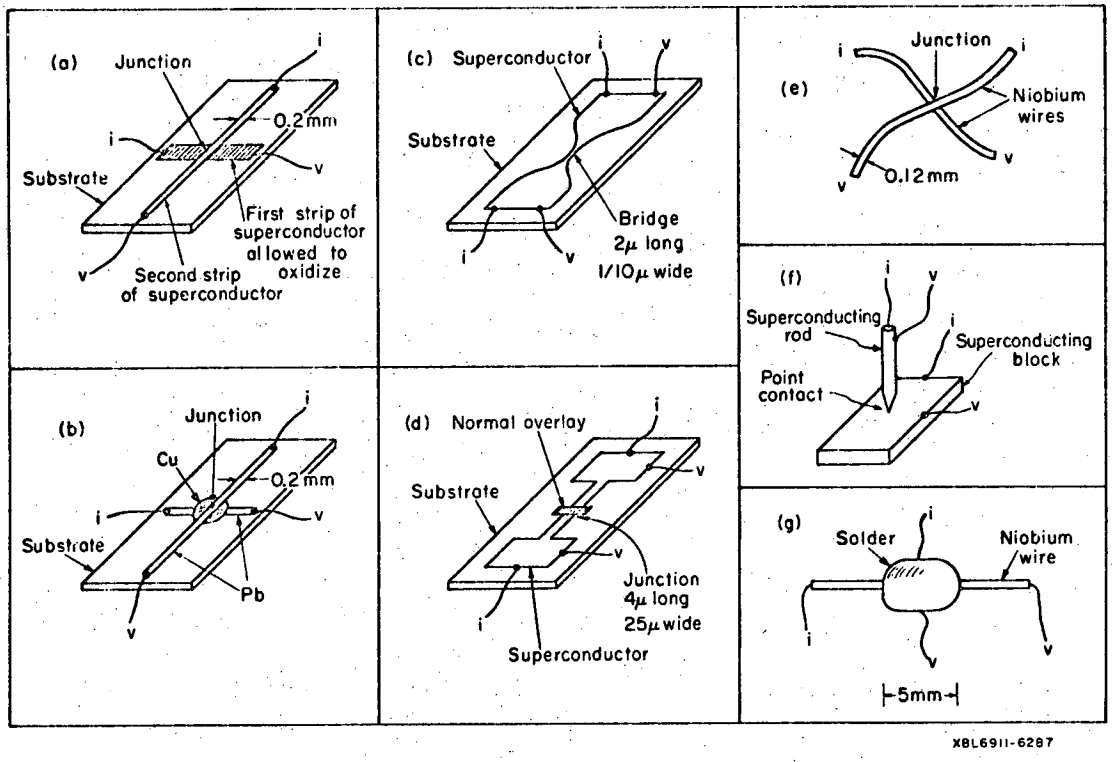
(a) Junction
i
0.2mm
i
v
Substrate
First strip of superconductor allowed to oxidize
v
Second strip of superconductor
(c) Superconductor
i
v
Substrate
Bridge
2μ long
1/10μ wide
i
v
(e) Junction
i
i
Niobium wires
0.12mm
v
v
(f)
i
v
Superconducting rod
i
Superconducting block
Point contact
v
(b) Junction
i
Cu
0.2mm
i
v
Substrate
Pb
v
(d) Normal overlay
i
Substrate
v
v
Junction
4μ long
25μ wide
i
Superconductor
(g) Solder
i
Niobium wire
i
v
v
5mm
XBL6911-6287

Fig. 1

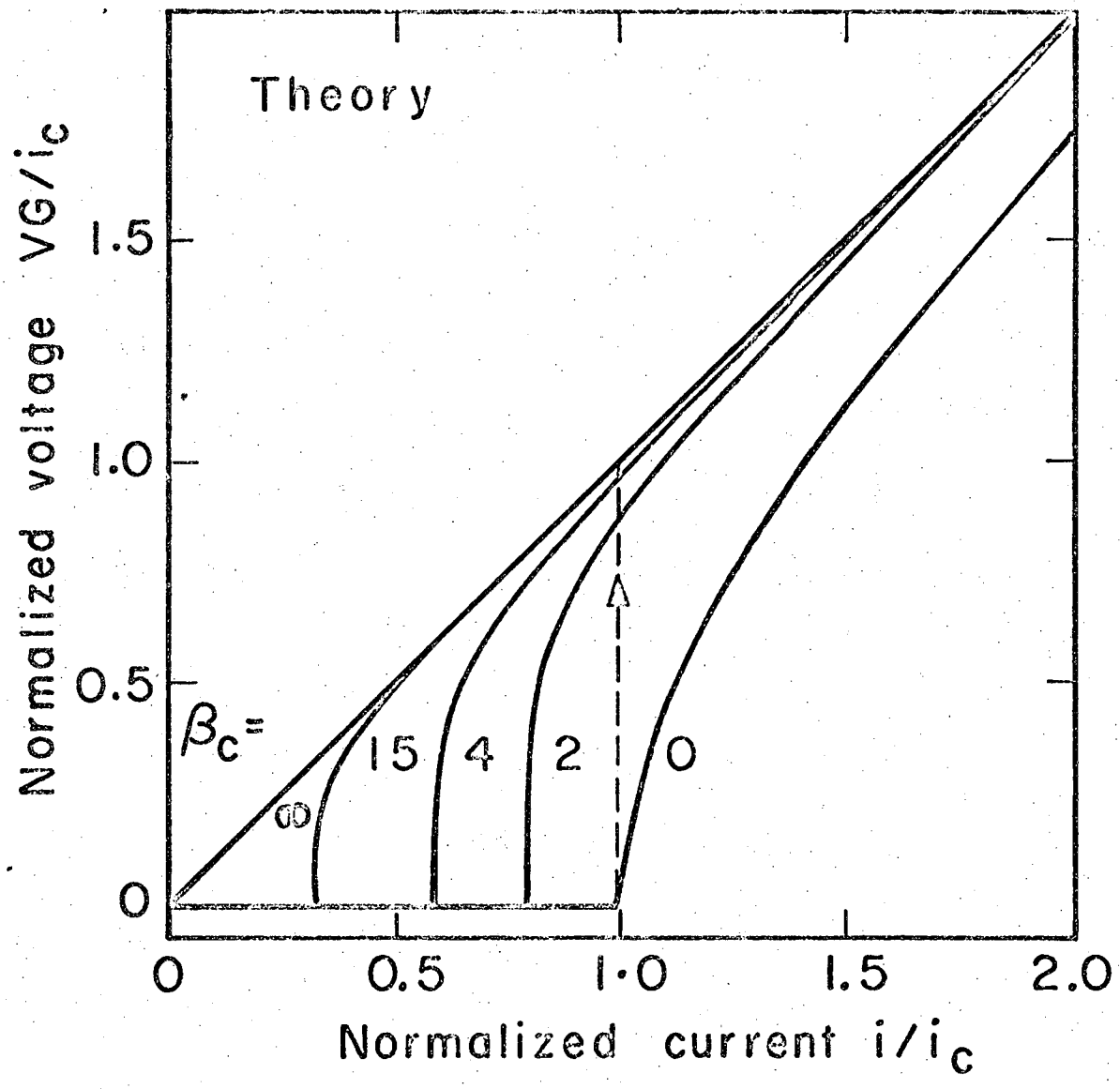

XBL715-3604

Fig. 2a

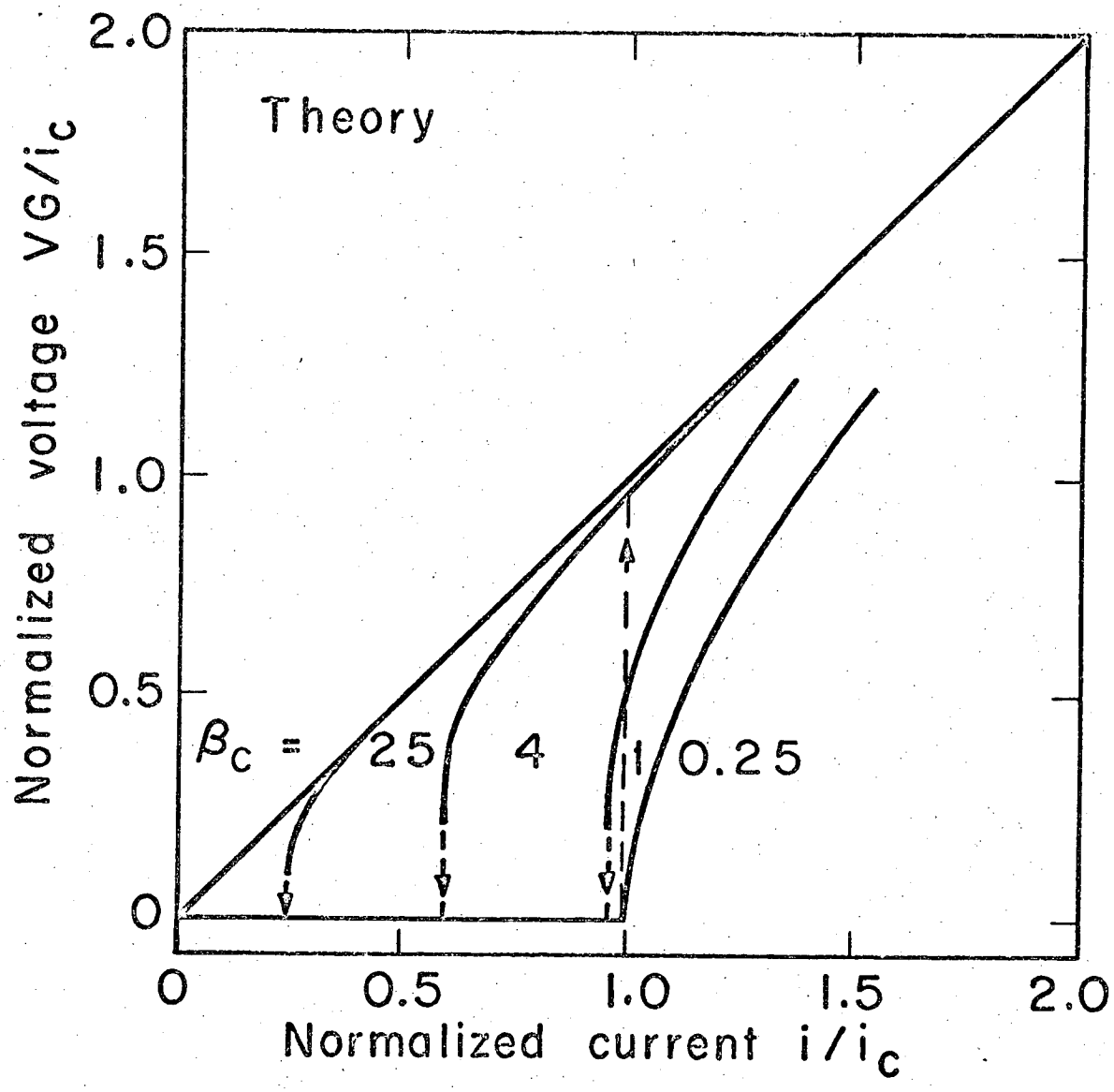

XBL715-3606

Fig. 2b

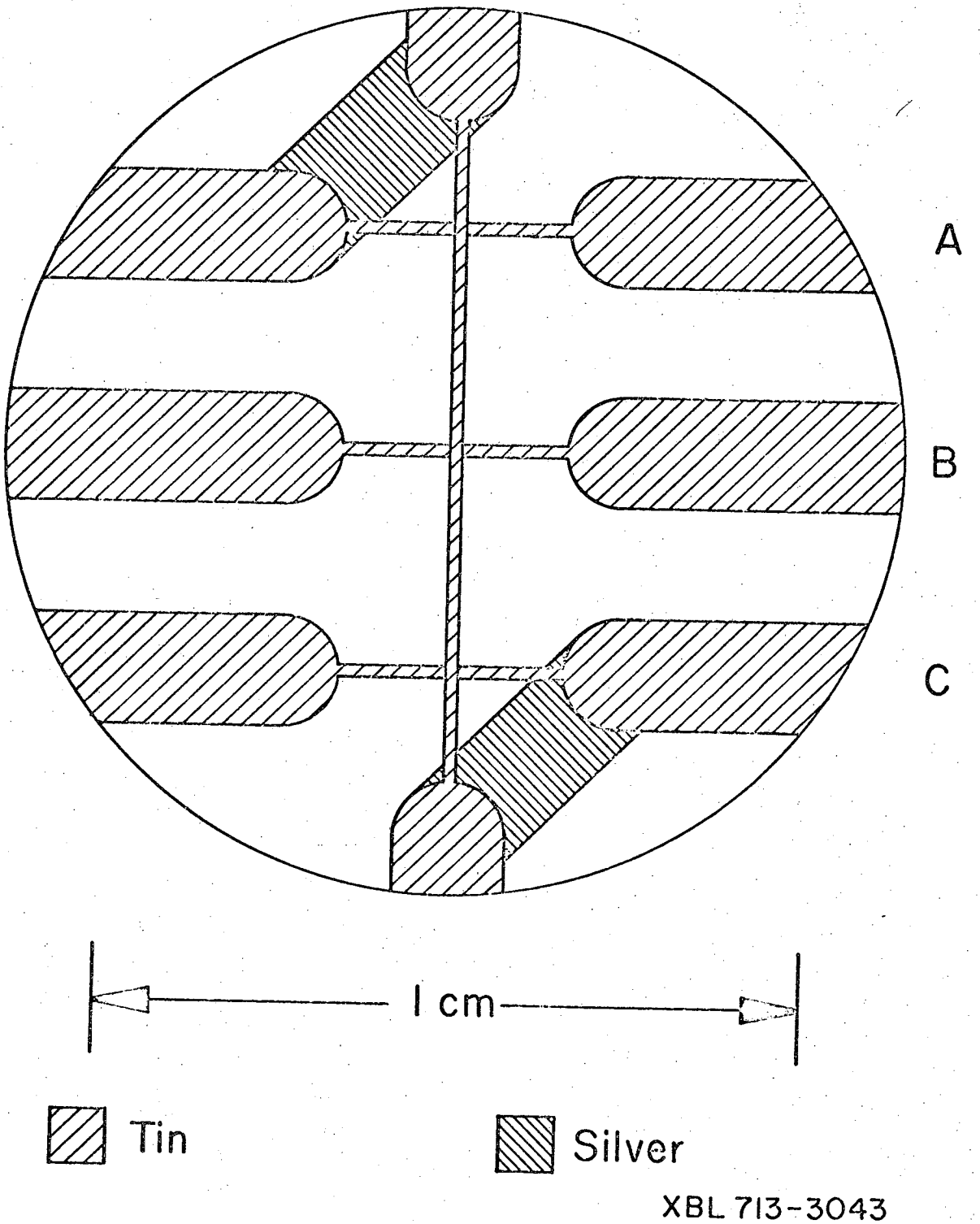

Fig. 3

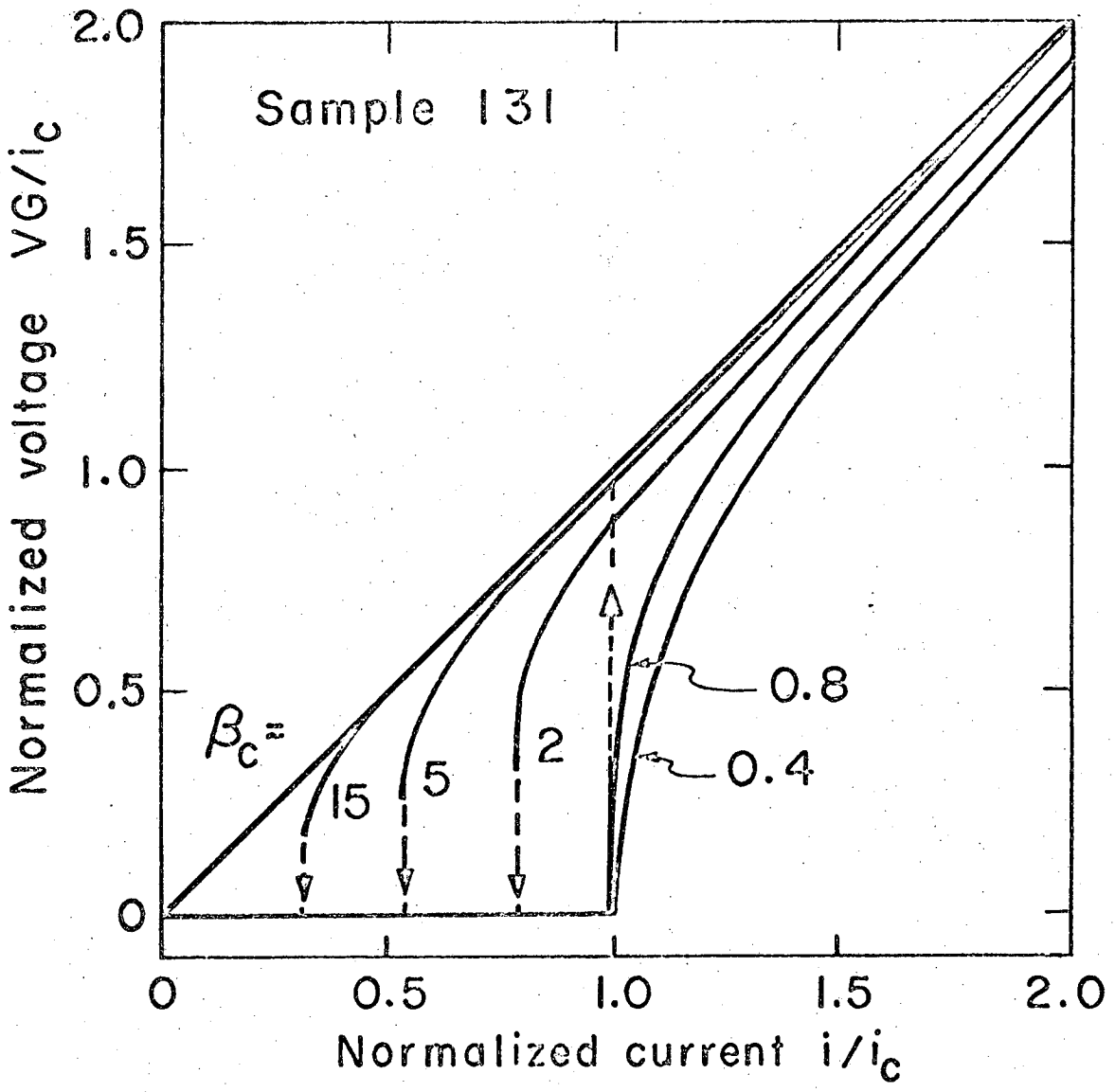

XBL715-3605

Fig. 4

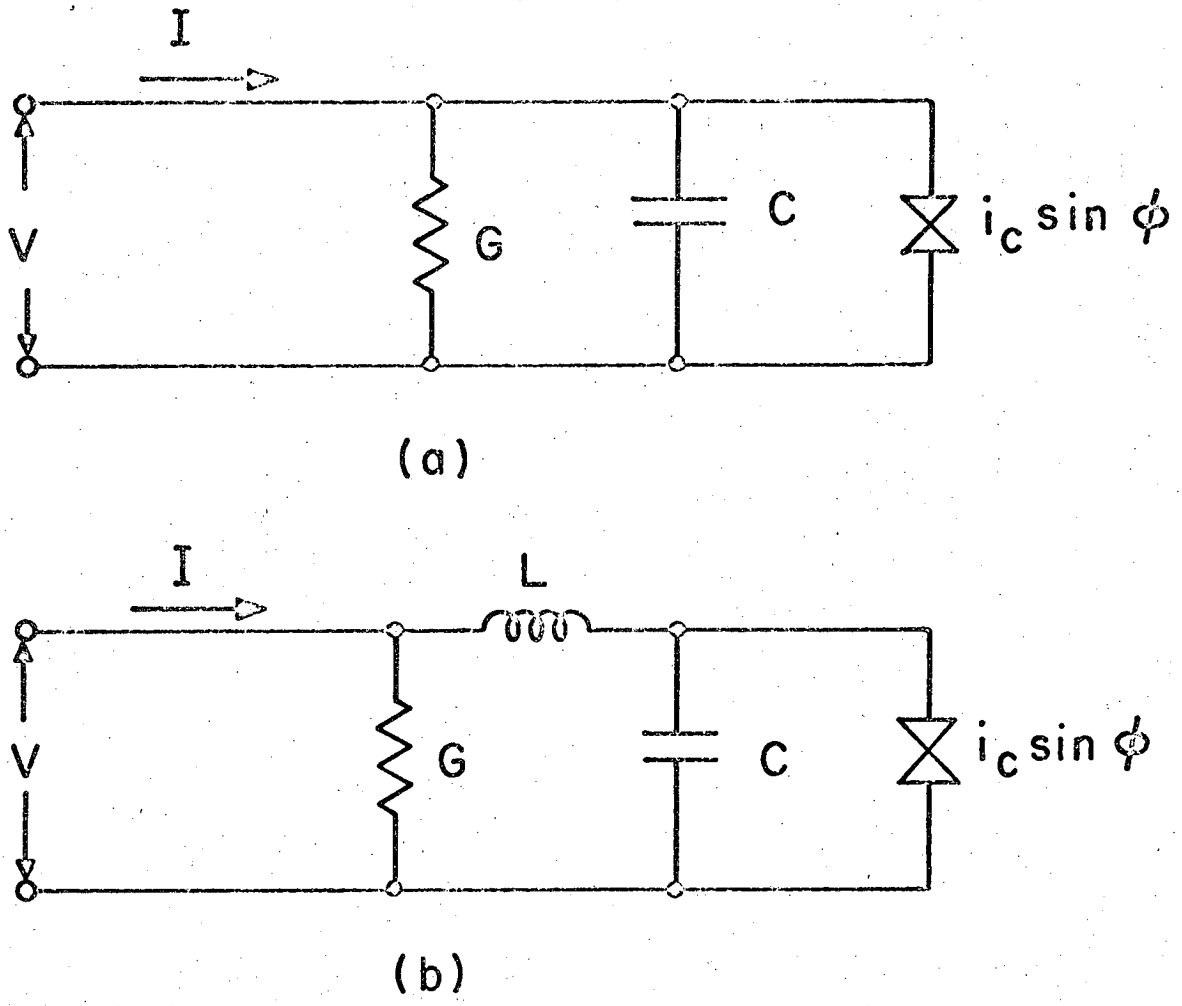

Fig. 5

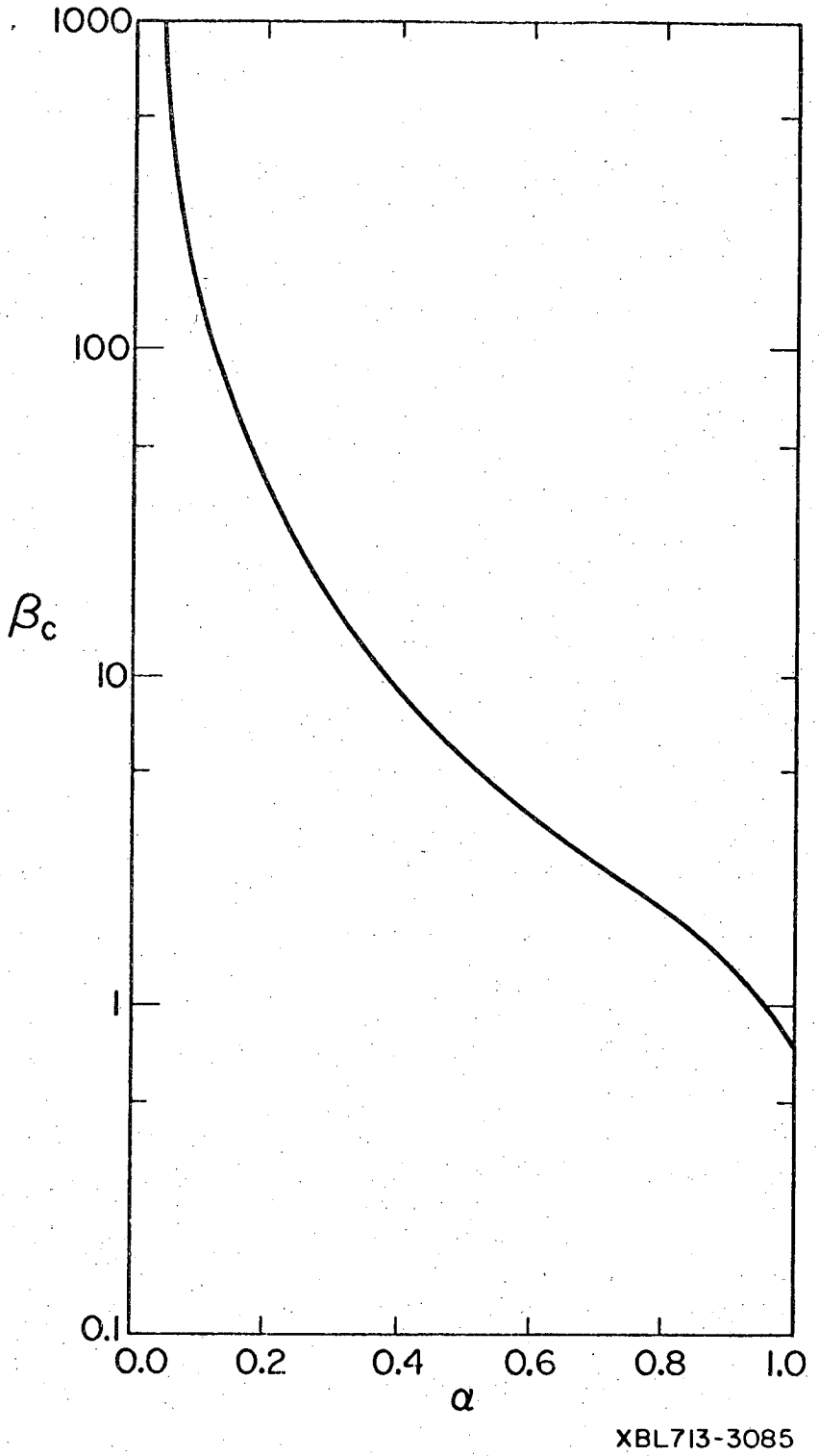

Fig. 6

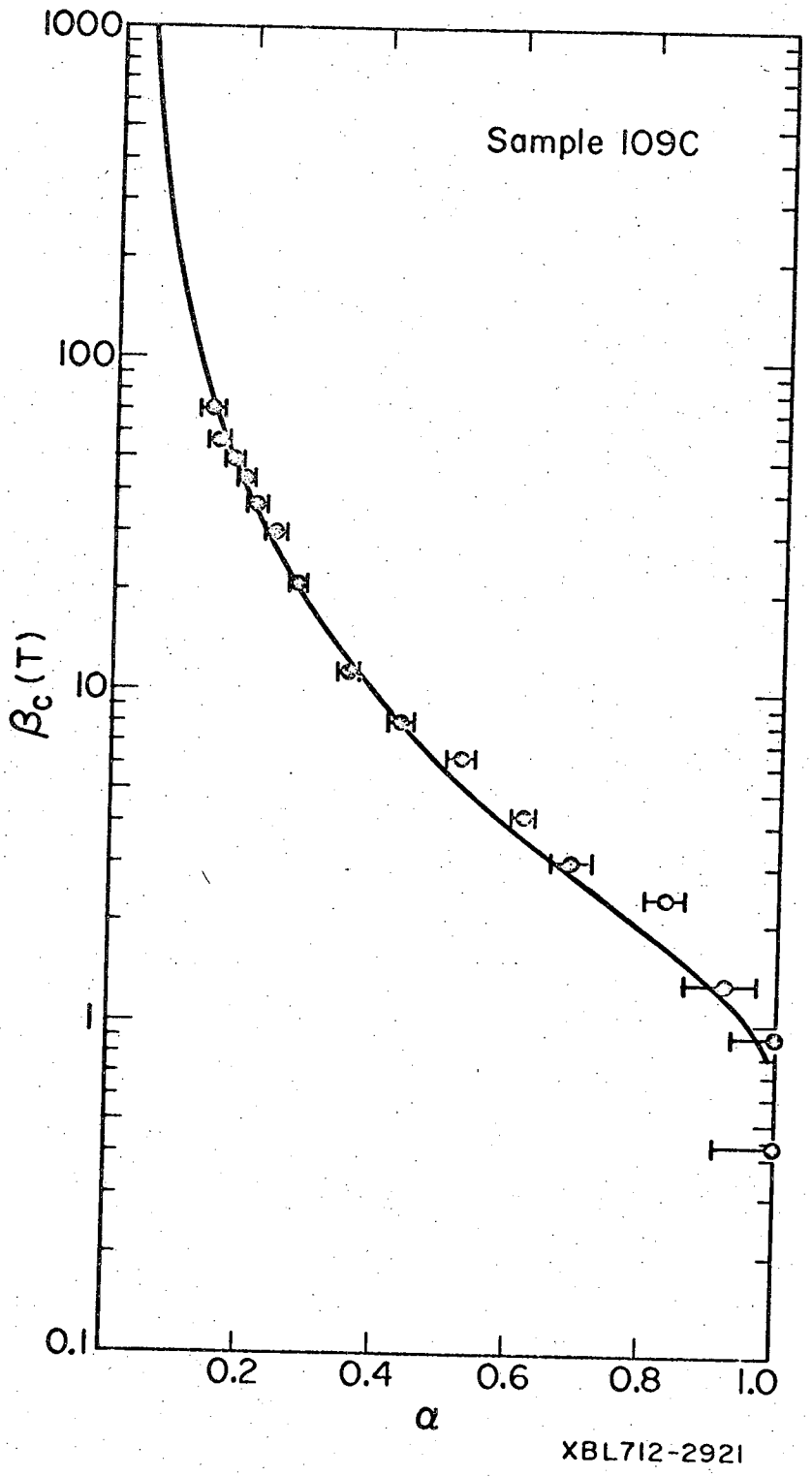

Fig. 7

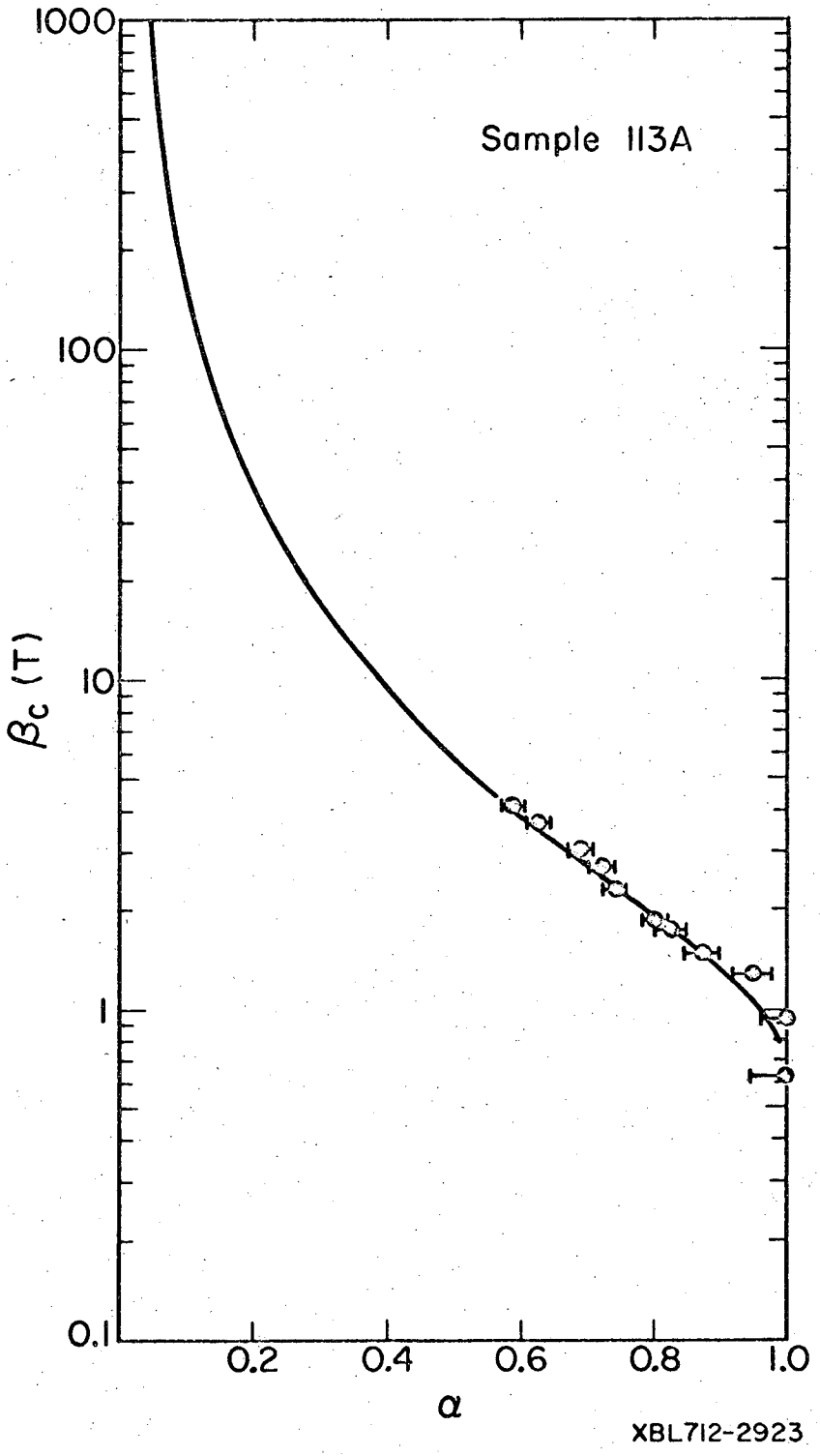

Fig. 8

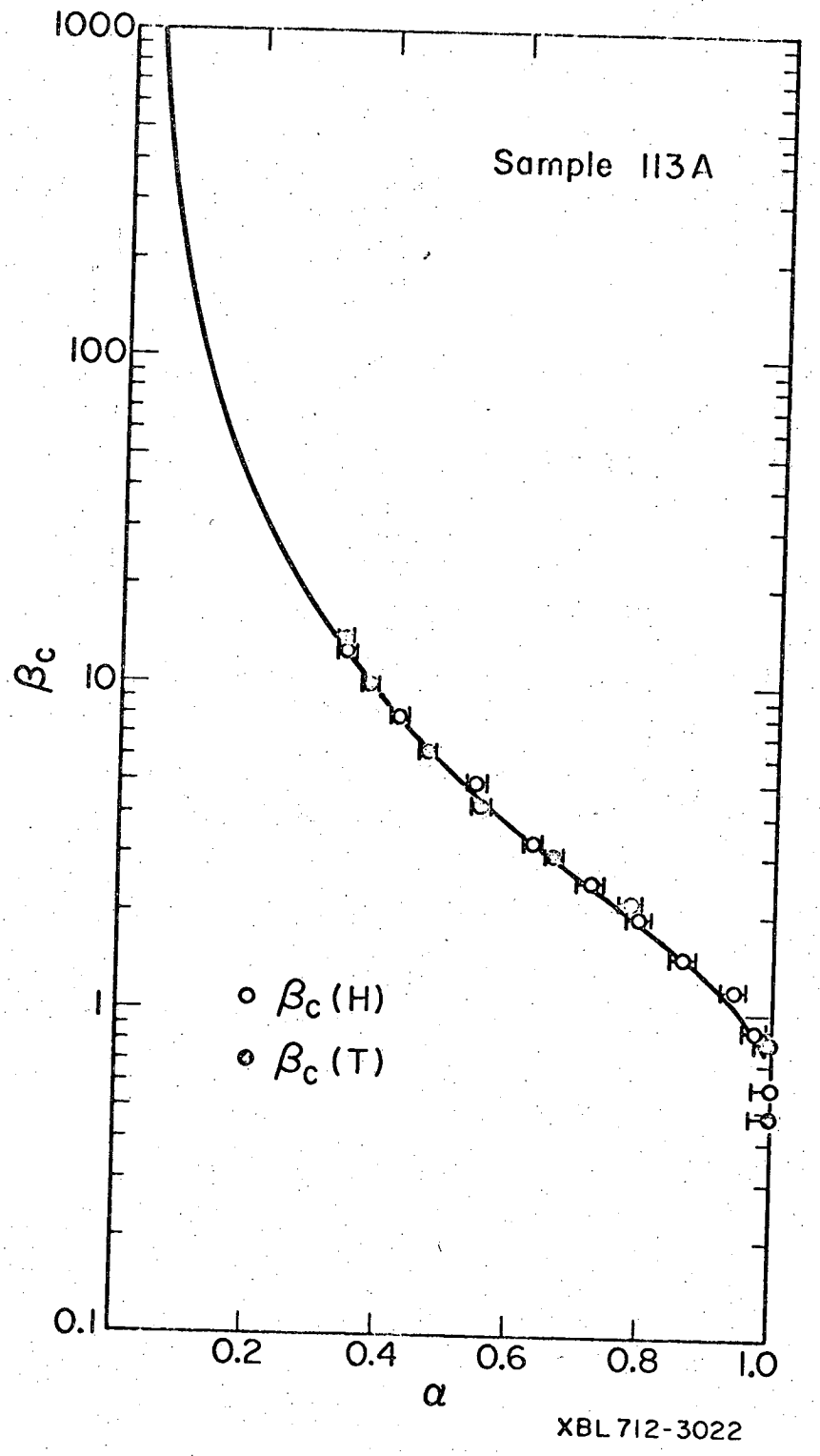
Sample 113A
1000
100
10
1
0.1
β_c
0.2
0.4
0.6
0.8
1.0
α
β_c (H)
β_c (T)
XBL 712-3022

Fig. 9

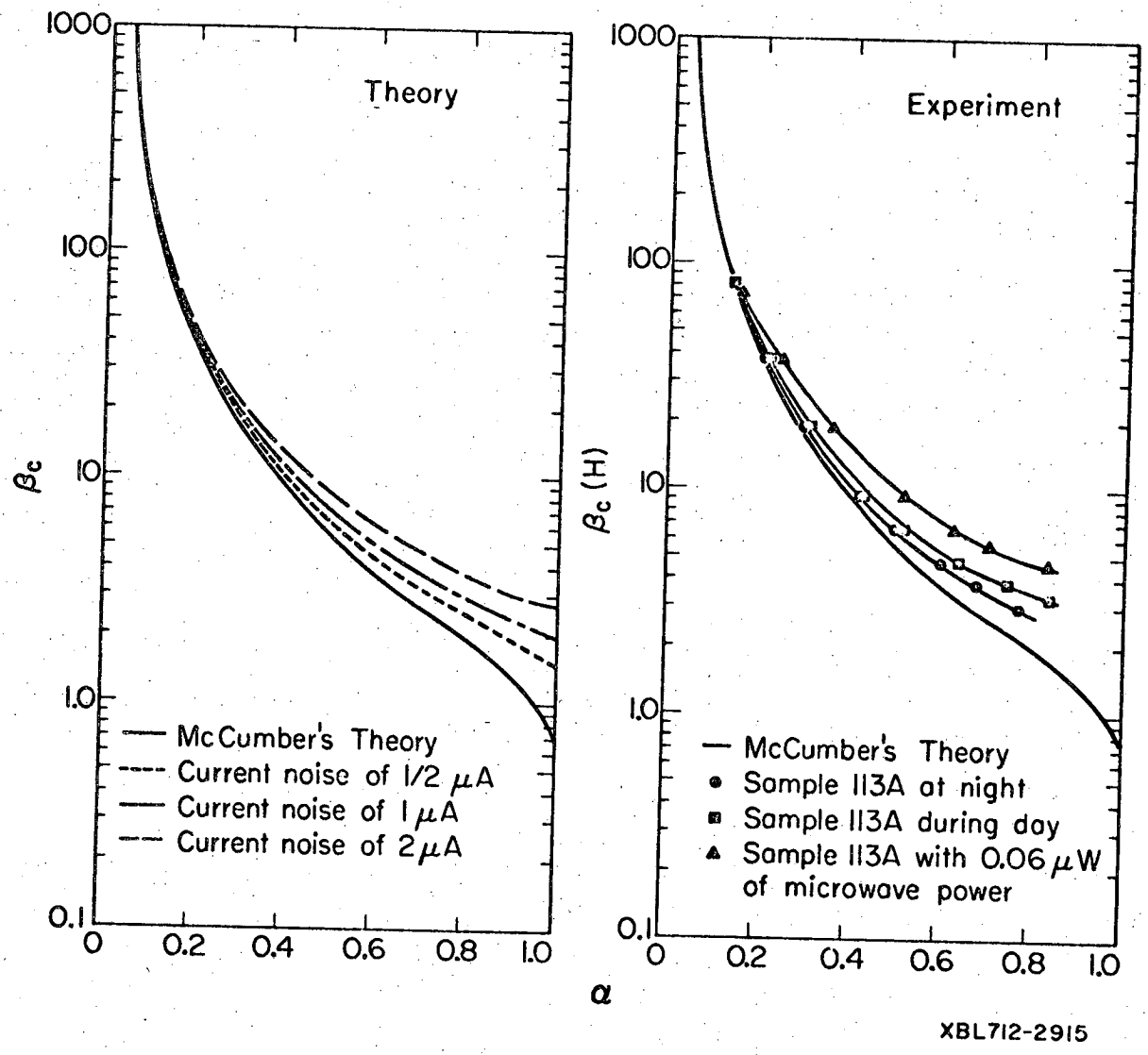
Theory
Experiment
β_c
β_c (H)
α
1000
100
10
1.0
0.1
0
0.2
0.4
0.6
0.8
1.0
McCumber's Theory
Current noise of 1/2 μA
Current noise of 1 μA
Current noise of 2 μA
McCumber's Theory
Sample 113A at night
Sample 113A during day
Sample 113A with 0.06 μW of microwave power
XBL712-2915

Fig. 10

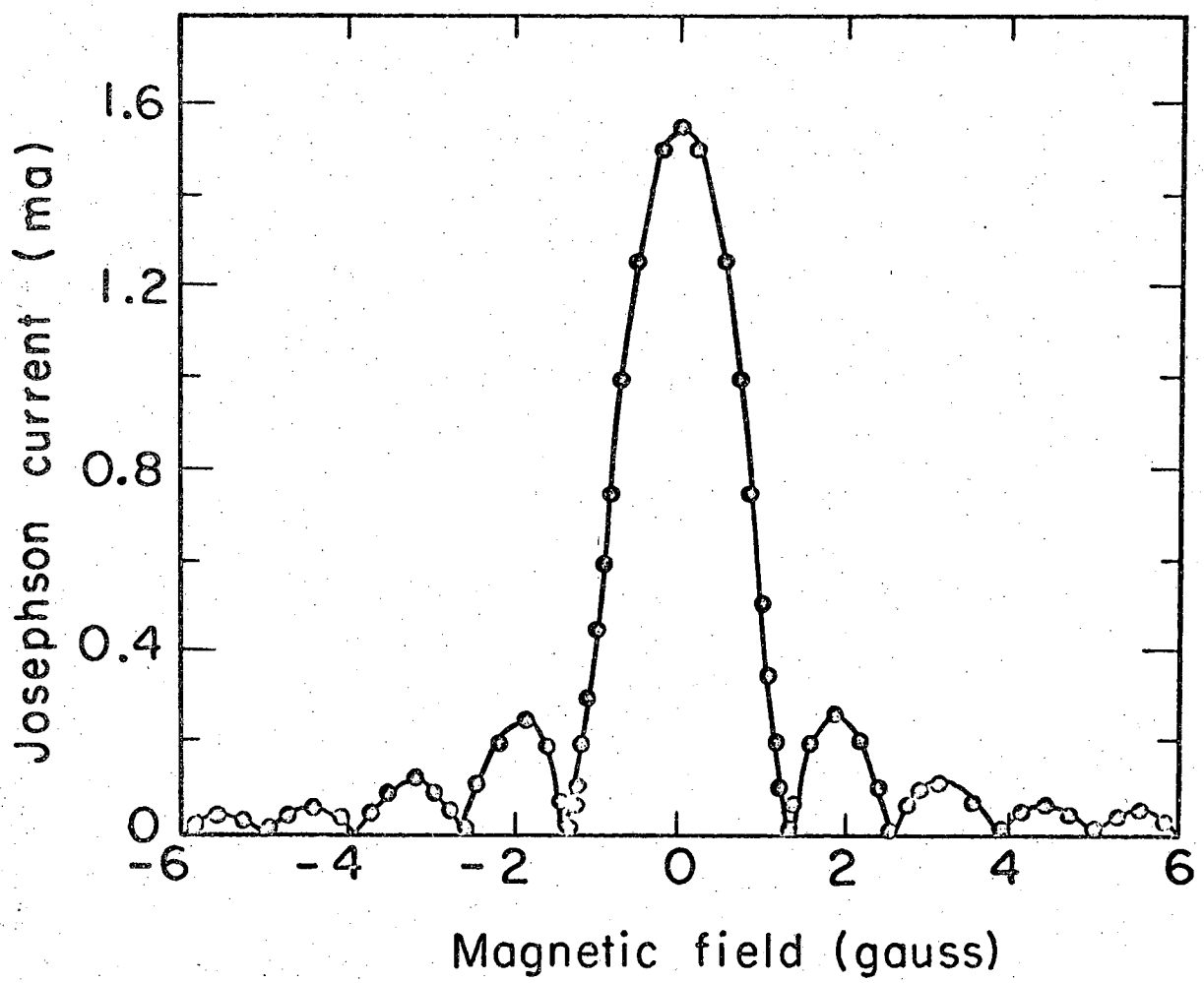

XBL712-2809

Fig. 11a

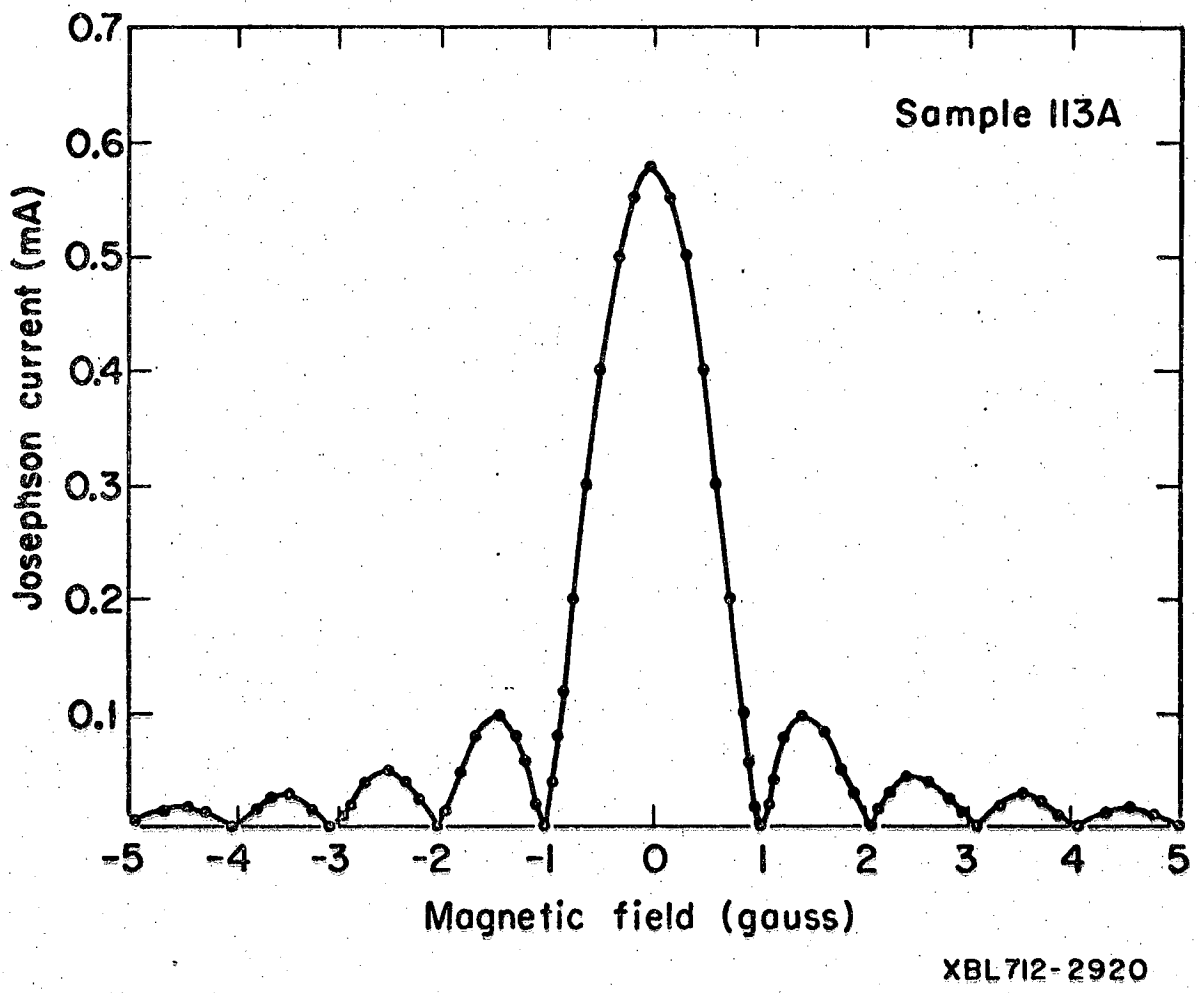
Sample 113A
Josephson current (mA)
0.7
0.6
0.5
0.4
0.3
0.2
0.1
-5
-4
-3
-2
-1
0
1
2
3
4
5
Magnetic field (gauss)
XBL712-2920

Fig. 11b